A Method for Assessing the Feasibility of Air-Bubble Screens to Reduce Morphological Gradients in Open-Channel Bends

Violaine Dugué
Laboratory of Hydraulic Constructions (LCH), Ecole Polytechnique Fédérale de Lausanne (EPFL), Switzerland. E-mail: violaine.dugue@gmail.com

Koen Blanckaert
State key, Laboratory of Urban and Regional Ecology, Research Center for Eco-Environmental Sciences, Chinese Academy of Sciences, Beijing, China. E-mail: koen.blanckaert@epfl.ch
Laboratory of Hydraulic Constructions (LCH), Ecole Polytechnique Fédérale de Lausanne (EPFL), Switzerland.

Qiuwen Chen
State key, Laboratory of Urban and Regional Ecology, Research Center for Eco-Environmental Sciences, Chinese Academy of Sciences, Beijing, China. E-mail: qchen@rcees.ac.cn

Anton J. Schleiss
Laboratory of Hydraulic Constructions (LCH), Ecole Polytechnique Fédérale de Lausanne (EPFL), Switzerland. E-mail: anton.schleiss@epfl.ch

ABSTRACT: The typical bar-pool bed topography which develops in open-channel bends due to complex interaction between streamwise flow, curvature-induced secondary flow, sediment transport and bed morphology leads to adverse impacts such as bed erosion near the outer bank that can endanger bank stability, and sediment deposition near the inner bank that can reduce the navigable width of the river. Previous experiments have shown that a bubble screen placed near the outer bank can produce a bubble-induced secondary flow that is able to redistribute the base flow pattern and consequently the bed morphology. The feasibility of the so-called bubble-screen technique is investigated in a sharply curved laboratory flume under different conditions of bed and sediment transport. Results of experiments performed on a fixed horizontal bed and on a mobile bed under both clear-water scour and live-bed conditions are compared. The bubble screen is found to be efficient if the maximum inward transverse velocities at the water surface produced by the bubble screen are higher than the maximal outward transverse velocities induced by the topographic steering and curvature-induced secondary flow. Moreover, this condition has to be satisfied all around the bend. Based on this criteria, a straightforward method to evaluate the efficiency of a bubble screen to redistribute the flow patterns and the morphology is proposed, and illustrated by means of an application case. The minimum air discharge required to counteract the maximal transverse velocities induced by the curvature is relatively low as compared to other types of environmental applications of the bubble screens.

KEY WORDS: Bubble screen, Erosion, Morphodynamics, Open-channel bend

1 INTRODUCTION

In the past decades, river engineering projects have shown a tendency towards more sustainable techniques. Preserving river ecomorphology and biodiversity while maintaining its principal economical functions calls for engineering techniques that intelligibly influence the fluvial system rather than forcing it.

This paper describes an innovative technique that consists in indirectly manipulating river morphology by provoking changes in the flow patterns. A bubble screen, originating from a porous tube located on the river bed, can generate a secondary flow perpendicular to the bubble-screen axis, called bubble-induced secondary flow (Fanneløp et al., 1991), which is able to redistribute the velocities and consequently to modify the bed morphology. The main advantage of this technique, contrary to "hard"

engineering techniques such as submerged groynes, riprap or bottom vanes, is that it does not imply a fixed construction on the river bed that can represents a threat for shipping, it has no visual impact, it is also reversible and can be used in a non-permanent way, for example only during high discharge events that may provoke scour. In open-channel bends, the bubble-screen technique can be used to generate a secondary flow that will counteract the curvature-induced secondary flow and thus decreases its effect on the morphological evolution of the bend. Figure 1 conceptually illustrates the working principle of the bubble screen in open-channel bends.

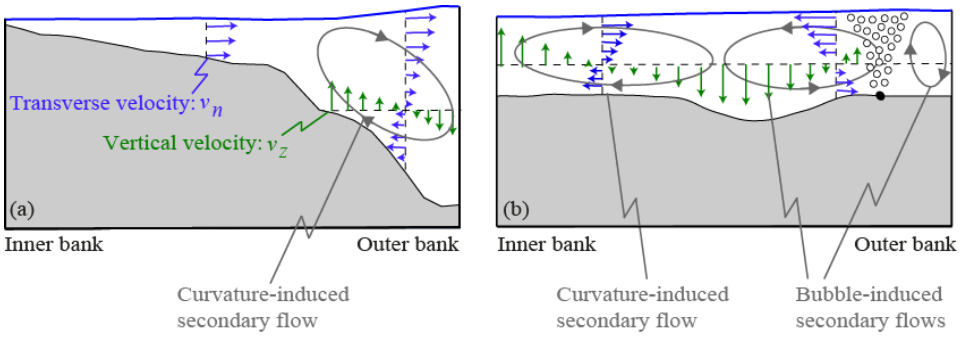

Figure 1 Conceptual sketch of (a) a reference case in an alluvial open-channel bend and (b) a case using the bubble-screen technique.

Based on knowledge and data available from literature, the fixed horizontal bed experiments by Blanckaert et al. (2008) and the mobile-bed experiments under clear-water scour conditions (Dugué et al., 2013) and under live-bed conditions (Dugué, 2013, Chapter 6), the present paper aims at developing a simple methodology for estimating the efficiency of the bubble-screen technique in a natural configuration.

2 EXPERIMENTS

Laboratory experiments were performed in a sharply curved flume of constant width B = 1.3 m with smooth vertical banks. The flume is composed of a 9 m long upstream straight reach, followed by a 193° bend with a constant centerline radius of curvature R = 1.7 m, and ended by a 5 m long downstream straight reach which includes a 2 m long sediment deposition basin. A curvilinear reference system (s, n, z) is adopted where the s-axis represents the streamwise direction, the transverse n-axis points in the outward direction and the vertical z-axis in the upward direction.

The sediment used as bed material was a quasi-uniform quartz sand with a mean diameter d_m = 0.002 m. When conducting experiments under live-bed conditions, sediment was continuously fed into the flume near the entrance by means of a back-and-forth moving scraper which controlled the sediment discharge. At the end of the flume, a sediment basin allowed for the deposition of the transported sediment.

The bubble screen was generated by means of a porous rubber tube (high-pressure tube of porous rubber, Multivis Waterbehandeling B. V.) with an inner diameter of 0.01 m, connected at both ends to a pressurized-air system to guarantee a quasi-constant air pressure on the entire length of the tube. Microscopic holes in the tube were located on opposite sides of the diameter with a longitudinal spacing of 0.003 m. The porous tube was ballasted on its whole length to avoid large-amplitude movements due to buoyancy effects, and was located at 0.2 m from the outer bank. During each experiment, the air pressure in the porous tube was controlled by means of a manometer and the air discharge measured by means of a rotameter.

Three types of experiments were performed with different bed and sediment transport conditions: Fixed Horizontal bed (FH), mobile bed under Clear-Water scour conditions (CW), mobile bed under Live-Bed conditions (LB). Experimental conditions are summarized in Table 1. More details about experiments are available in Dugué (2013).

At morphologic equilibrium, patterns of the three-dimensional velocity vector and the turbulence

were measured in several cross-sections around the bend by means of an Acoustic Doppler Velocity Profiled (ADVP) (Lemmin and Rolland, 1997; Hurther and Lemmin, 1998; Blanckaert, 2010). Vertical velocity profiles were measured in the investigated cross-sections every 0.05 m in the range n = –0.45 m to n = 0.40 m. ADVP measurements were not possible in the vicinity of the bubble screen because of interferences between air-bubbles and the acoustic signal. Water surface elevation was measured with a point gauge and bed elevation was measured with a laser distometer in cross-sections every 5° in the bend with a transverse spacing of 0.05 m.

Table 1 Experimental conditions

Label	Q $[m^3 s^{-1}]$	q_s $[kg\ m^{-1} s^{-1}]$	H $[m]$	U $[m\ s^{-1}]$	Fr $[-]$	q_a $[dm^3 s^{-1} m^{-1}]$	R/H $[-]$	B/H $[-]$
CF89_FH_NB	0.089	-	0.16	0.43	0.34	-	10.7	8.2
CF89_FH_B	0.089	-	0.16	0.43	0.34	0.16	10.7	8.2
CF57_CW_NB	0.057	-	0.14	0.31	0.26	-	11.9	9.1
CF55_CW_B	0.055	-	0.14	0.31	0.26	0.21	12.2	9.3
CF75_LB_NB	0.075	0.025	0.14	0.41	0.35	-	12.1	9.2
CF75_LB_B	0.075	0.025	0.14	0.41	0.35	0.24	12.1	9.2

Q is the water discharge, q_s the sediment discharge per unit width, H the flume-averaged water depth, $U = Q/(BH)$ the flume-averaged velocity, $Fr = U/\sqrt{gH}$ the flume-averaged Froude number, q_a the air discharge per unit length of porous tube. The first part of the experiments' labels refers to Curved Flow (CF) with the water discharge in [l s^{-1}], the second part fixed horizontal bed (FH), live-bed (LB) or clear-water scour (CW) conditions, and the last part experiments without (NB) or with (B) bubble screen.

3 MORPHOLOGY

Figure 2 shows the final bed morphology in the experiments under clear-water scour and live-bed conditions without (Figure 2a and Figure 2b) and with (Figure 2c and Figure2d) the bubble screen.

In the two reference experiments (Figure2a and Figure2b), the typical bar-pool bed topography is observed with a shallow point bar near the inner bank and two main scour holes near the outer bank: the first one near the bend entry between the cross-sections at 40 and 100°, and the second one near the bend exit around the cross-section at 180° (Odgaard, 1981; Dietrich and Smith, 1983; Blanckaert, 2010).

The bed morphologies in reference tests with and without sediment feeding are not significantly different. In the clear-water scour experiment (Figure 2a), no sediment comes from upstream. Consequently, the morphology only develops due to bend effects. The curvature-induced secondary flow redistributes the flow and causes the bed shear stress to be higher than the critical bed shear stress in some parts of the bend. At the end of the experiment, sediment transport totally vanishes. This leads to the development of a point bar at the inner bend and to erosion near the outer bank. A very similar morphology develops in the reference experiment under live-bed conditions CF75_LB_NB (Figure 2b). The main difference comes from migrating mobile bedforms under live-bed conditions, which can be identified by the small scour holes near the outer bank. However, they do not affect the large-scale bar-pool bed topography.

Under clear-water scour conditions, the bubble screen dramatically modifies the bed morphology all around the bend (Figure 2c). The maximum scour hole between the cross-sections at 40° and 100° is shifted from the outer bank towards the center of the flume and its depth has been reduced by about 50%. The bed level is in general much flatter than in the reference experiment and the second scour hole at the bend exit does not develop.

Under live-bed conditions (Figure 2d), the bubble screen technique has a favourable influence only in the second part of the bend. Indeed, the second scour hole is considerably reduced and shifted from the outer bank to the middle of the cross-section. However, in the upstream part of the bend, the first scour hole and the point bar are still observed.

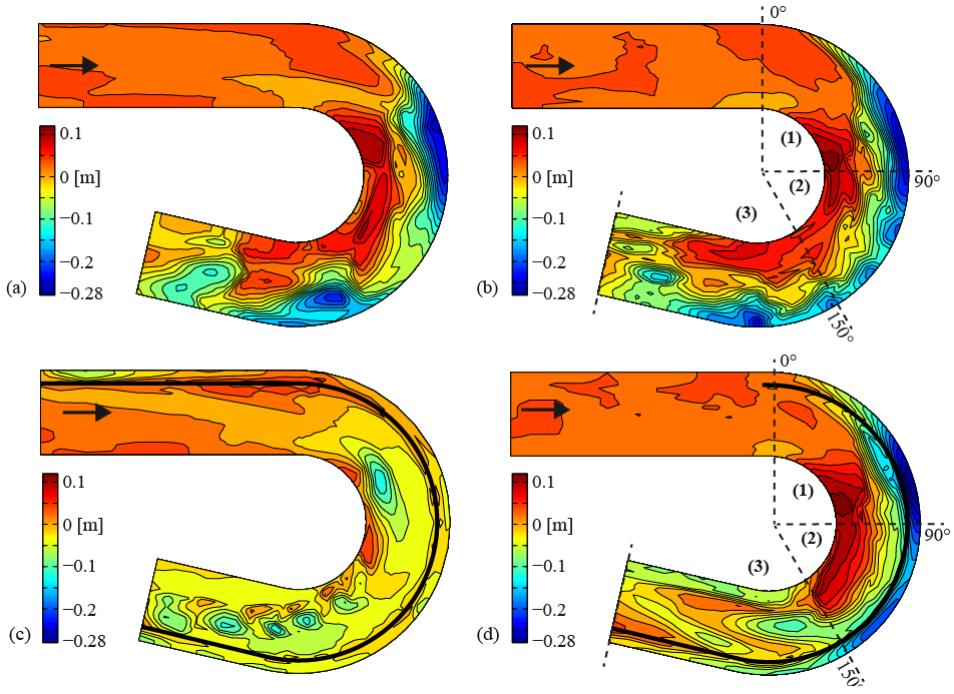

Figure 2 Equilibrium bed morphology from laser altimetry measurements for the reference experiments without bubble screen CF57_CW_NB (a) and CF75_LB_NB (b), the bubble screen experiments CF55_CW_B (c) and CF75_LB_B (d). Isolines are shown with an interval of 0.02 m. The same color scale has been used to facilitate comparison. Three zones in the live-bed experiments refer to Dugué (2013): (1) no bubble-induced secondary flow cell; (2) bubble-induced secondary flow cell causing velocity redistribution; (3) bubble-induced secondary flow cell causing velocity and morphology redistributions.

4 FLOW PATTERNS

The measured flow patterns reveal why the bubble-screen technique is efficient in redistributing the bed morphology in the second part of the bend in the live-bed experiment, and why it is rather ineffective in the upstream part of the bed (Figure 2). The pattern of secondary flow is the key to understand and explain the effect of the bubble-screen on the morphology. The signature of the secondary flow pattern is well illustrated by the patterns of the transverse velocities at the water surface, $v_{n,surf}$. Figure 3 compares these patterns in fixed horizontal bed and live-bed experiments with and without bubble screen.

In the CF89_FH_NB experiment over fixed horizontal bed without bubble screen (Figure 3a), a curvature-induced secondary flow cell exists all around the bend, as indicated by the outwards velocities at the water surface. Over the fixed horizontal bed (Figure 3b), a bubble-induced secondary flow with inward velocities at the water surface is observed all around the bend, and the curvature-induced secondary flow is shifted inwards. The size of the bubble-induced secondary flow increases in downstream direction, and is similar to observations in straight flow experiments (Dugué, 2013, Chapter 4). The bubble-induced secondary flow cell extents from n = 0.1 m to n = 0.45 m in the cross-section at 60°, and from n = –0.1 m to n = 0.45 m to half the cross-section at 180° in the bend.

In the CF75_LB_NB experiment with live-bed and without bubble screen (Figure 3c), the bed topography leaves a strong footprint on the distribution of $v_{n,surf}$. Topographic steering of the flow (Nelson 1988; Blanckaert 2010) towards the deepest regions in the flow domain (Figure 2b) causes strong outward velocities towards the two scour holes (Figure 3c). This pronounced topographic steering is due to the abrupt change in centerline curvature at the bend entrance and exit. The bubble-induced secondary flow cannot overcome the topography-induced strong outwards velocities in the first part of the bend (Figure 3d). As a result, the bubble-screen is unable to redistribute flow and morphology patterns in the first part of the bend (Figure 2d). The middle part of the bend is representative of bends with gradual change in curvature, and associated reduced topographic steering. In this region, the bubble-induced secondary flow

comes into existence and amplifies in downstream direction (Figure 3d). It is efficient in influencing the bed morphology (Figure 2d). In the cross-sections at 180°, the bubble-induced secondary flow size is similar in CF89_FH_B and CF75_LB_B experiments.

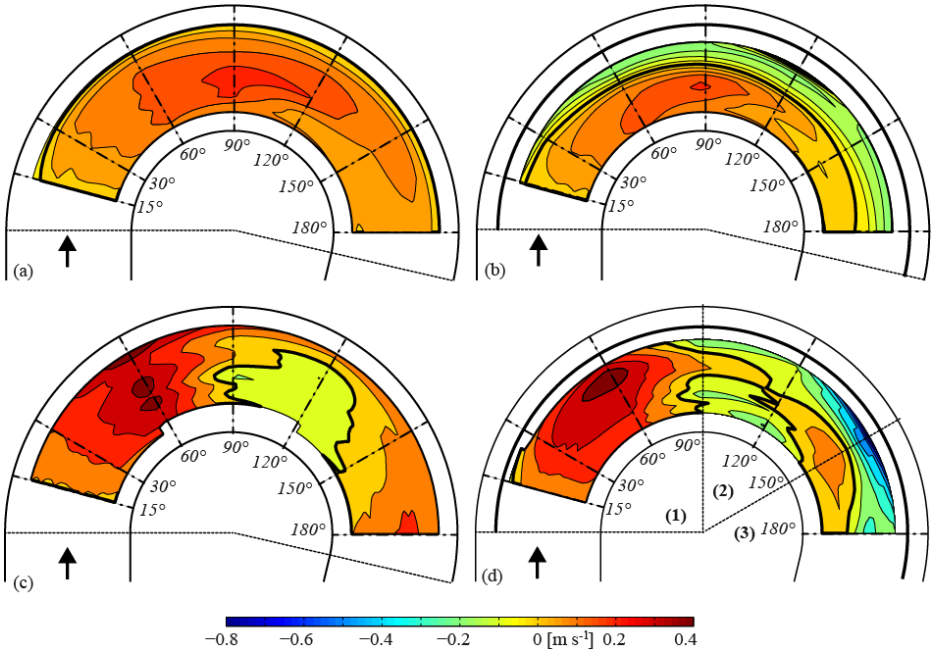

Figure 3 Transverse velocity at the water surface, $v_{n,surf}$, based on ADVP measurements in the indicated cross-sections in CF89_FH_NB (a), CF89_FH_B (b), CF75_LB_NB (c) and CF75_LB_B (d) experiments. The same color scale has been used to simplify comparison.

5 FEASIBILITY OF THE BUBBLE-SCREEN TECHNIQUE

The above results indicate that the efficiency of the bubble-screen technique can be estimated by comparing the transverse velocities at the water surface induced by topographic steering and by the bubble screen. The bubble screen will only be able to modify the morphology all around the bend if it is able to overcome the topographic steering near the bend entrance induced by the increase in centerline curvature. In first approximation, this condition is satisfied if the bubble-induced transverse inwards velocities at the water surface, $v_{n,surf,bub}$, are strong enough to counteract the curvature-induced transverse outward velocities at the water surface in the reference situation without bubble screen, $v_{n,surf,ref}$:

$$\max\left(-v_{n,surf,bub}\right) > \max\left(v_{n,surf,ref}\right) \tag{1}$$

5.1 Estimation of max($-v_{n,surf,bub}$)

Different analytical models give estimations of the maximal value of $v_{n,surf,bub}$, based on the flow depth, air discharge and several empirical parameters under still water conditions (Milgram, 1983, Wen and Torrest, 1987, Fanneløp et al., 1991, Riess and Fanneløp, 1998, Brevik and Kristiansen, 2002). Maximum transverse surface velocities produced by a bubble screen, under still-water conditions, can be straightforwardly determined based on Brevik's formula, which does not include empirical parameters (Brevik, 1977, Brevik and Kristiansen, 2002):

$$\max\left(v_{n,surf,bub}\right) = 1.7\left(gq_a\right)^{1/3}\left(1+\frac{H}{H_a}\right)^{-1/3} \tag{2}$$

where H_a [m] is the atmospheric pressure head, H [m] the water depth, and q_a [m^3 s^{-1} m^{-1}] the air discharge. The atmospheric pressure is expressed as the equivalent of 10 m high water column. The experiments of Wen and Torrest (1987) agree well with this formula.

Figure 4 compares measurements of $v_{n,surf,bub}$ in a straight laboratory flume under still water and straight flow conditions (Dugué 2013, chapter 4) to the theoretical estimation according to Brevik's formula (Eq. 2). The same air discharge (q_a = 0.24 dm^3 s^{-1} m^{-1}) was used for all the investigated tests. In the range of investigated flow depths (H from 0.11 m to 0.21 m), the water depth is found to have no influence on max($v_{n,surf,bub}$). Moreover, under straight flow conditions, the bubble-induced flow structures were not influenced by the base flow velocity, which mainly advects the bubble-induced secondary flow in downstream direction. Brevik's formula predicts a value of max($v_{n,surf,bub}$) = 0.23 m s^{-1} which is lower than the measured velocities at the same distance from the bubble screen max($v_{n,surf,bub}$) = 0.33 m s^{-1}. This suggests that Brevik's formula provides a conservative estimate of max($v_{n,surf,bub}$).

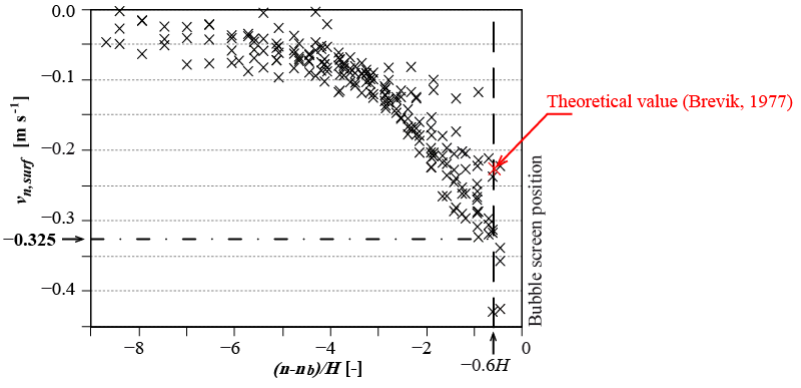

Figure 4 Transverse profile of $v_{n,surf,bub}$ based on measurements in still water and straight flow conditions (Dugué, 2013, Chapter 4). n_b is the location of the porous tube. Measurements were performed with H = 0.11; 0.16 and 0.21 m and q_a = 0.24 dm^3 s^{-1} m^{-1}. Comparison with the theoretical value from Brevik (1977).

The minimum air discharge required to generate a bubble-screen induced secondary flow that is strong enough to overcome topographic steering effects according to Eq. 1 can be estimated by reformulating Brevik's formula (Eq. 2) as:

$$q_{a,\min} = \left(\frac{1}{1.7}\max\left(v_{n,surf,ref}\right)\right)^3 \frac{1}{g}\left(1+\frac{H}{H_a}\right) \tag{3}$$

The operating cost of the bubble screen mainly depends on the energy expended by the air compressor, which depends on the air discharge (Sahoo and Luketina, 2006). Therefore, Eq. 3 provides the basis for evaluating the minimum cost of the required installation and determining the economic feasibility of the bubble-screen technique.

5.2 Estimation of max($v_{n,surf,ref}$)

The maximum value of $v_{n,surf,ref}$ can be estimated by direct measurements of the 3-D flow patterns in the concerned river (Frothingham and Rhoads, 2003, Blanckaert et al., 2009, Nanson, 2010, Engel and Rhoads, 2012, Sukhodolov, 2012). However, field measurements are mostly not feasible during high-flow conditions which are mainly responsible for the river morphological development.

Modeling of three-dimensional flow field in a curved channel can be performed by means of large-eddy simulation (LES) (van Balen et al., 2009, van Balen et al., 2010a, van Balen et al., 2010b) or Reynolds-averaged numerical simulations (RANS) (Zeng et al., 2008; van Balen et al., 2010a). However, these models require detailed input information of the bathymetry and are often time-consuming and computationally too expensive when applied to real river configurations (Rüther and Olsen, 2007, Fischer-Antze et al., 2008).

A straightforward first assessment of the maximum transverse velocity at the water surface can be obtained with reduced-order models for the flow and the morphology. These models adopt hypotheses that allow for simplifying the three-dimensional Navier-Stokes equations and transforming them into a system of coupled first-order differential equations. Such models have been progressively developed and

refined during the last decades (Ikeda et al., 1981; Odgaard, 1989; Johannesson and Parker, 1989; Zolezzi and Seminara, 2001; Blanckaert and de Vriend 2003, 2010) These models can be presented in a general mathematical framework that parameterizes the morphology, and patterns of the main flow, the curvature-induced secondary flow and the secondary flow induced by topographic steering.

The bed morphology is parameterized by means of the scour factor *A/R*, which represents the transverse bed slope.

$$\frac{A}{R} = -\frac{1}{H_w}\frac{\partial z_b}{\partial n} \tag{4}$$

The elevation of the bed level is indicated by z_b, and H_w is the cross-sectional averaged flow depth. The scour factor varies in downstream direction. It can be determined based on field measurements or it can be computed by means of a reduced-order model (de Vriend and Struiksma, 1984; Odgaard, 1989; Zolezzi and Seminara, 2001; Camporeale et al., 2007; Ottevanger et al., 2013).

The transverse profile of the depth-averaged streamwise velocity, U_s, is parameterized as:

$$\frac{\alpha_S}{R} = \frac{1}{U_S}\frac{\partial U_S}{\partial n} \tag{5}$$

Secondary flow induced by topographic steering is represented by the depth-averaged transverse velocity U_n, whereas secondary flow induced by the curvature is represented by v_n^*. Reduced-order models provide solutions for α_s, U_n and v_n^*, which allow assessing the maximum transverse velocity at the water surface, $\max(v_{n,surf,ref})$.

Obviously, the accurate estimation of the curvature-induced secondary flow is the key component in the present application. Most reduced-order models for curved flow are based on the assumption of mild curvature and mild variations in curvature. They predict the transverse velocity to increase proportionally with the curvature ratio *H/R* as:

$$v_n^* = \frac{U_w H_w}{R} f_{n,0}(C) \tag{6}$$

where C is the Chézy friction coefficient and $f_{n,0}$ is a function that represents the vertical profiles of v_n^*. Solutions for $f_{n,0}$ have been reported by Rozovskii (1957) and de Vriend (1977).

This mild-curvature model is known to overestimate the magnitude of the curvature-induced secondary flow. Indeed, a non-linear feedback exists between the streamwise and secondary flows which reduces the magnitude of the secondary flow (de Vriend, 1981, Yeh and Kennedy, 1993). This non-linear feedback is integrated in the non-linear model of Blanckaert and de Vriend (2003, 2010) which predicts the curvature-induced transverse velocity as:

$$v_n^* = U_w H_w \left[\left(\frac{\sqrt{f_n^2}}{R} \right) \frac{1}{\sqrt{f_{n,0}^2}} \right] f_{n,0} \tag{7}$$

where the term between square brackets provides a correction factor for the mild-curvature solution (Eq. 7). This correction factor is provided by Blanckaert and de Vriend (2003). Finally, the non-linear model of Blanckaert and de Vriend (2003, 2010) predicts $\max(v_{n,surf,ref})$ as:

$$\max\left(v_{n,surf,ref}\right) = U_n + U_w H_w \left(\frac{\sqrt{f_n^2}}{R} \right) \frac{1}{\sqrt{f_{n,0}^2}} f_{n,0,\max}(C) \tag{8}$$

This non-linear model without curvature restrictions has been validated for strongly-curved laboratory flumes with fixed horizontal bed and live-bed, as well as natural alluvial rivers (Blanckaert and de Vriend 2003; 2010; Ottevanger et al. 2012), and was shown to improve considerable predictions of the main and secondary flow distributions.

Blanckaert and de Vriend's model (2003; 2010) has been applied to CF89_FH_NB and CF75_LB_NB experiments. In the mobile bed experiment, *A/R* has been derived from the detailed topographic measurements.

Table 2 summarizes the solutions for max($v_{n,surf,ref}$) resulting from the non-linear modeling of the CF89_FH_NB and CF75_LB_NB experiments. Compared to the experimental results, the non-linear model underestimates max($v_{n,surf,ref}$) by 27% and by 4 % in CF89_FH_NB and CF75_LB_NB experiments, respectively. The simulations give a satisfactory estimation of max($v_{n,surf,ref}$) with only few required input parameters, especially in the case of a mobile bed.

Table 2 Comparison of linear-model and non-linear model results with experimental data.

Label				Experiments	Non-linear model
	Q	H/R	$C/\sqrt{g}$	$max(v_{n,surf,ref})$	max($v_{n,surf,ref}$)
	$[m^3\ s^{-1}]$	[-]	[-]	$[m\ s^{-1}]$	$[m\ s^{-1}]$
CF89_FH_NB	0.089	0.093	11.7	0.22	0.16
CF75_LB_NB	0.075	0.083	11.4	0.47	0.45

6 APPLICATION TO NATURAL RIVER

The method to assess the feasibility of an air-bubble screen is applied to three sharply curved bends on the Ledra river (Italy, Figure 5) which were investigated by Blanckaert et al. (2009). Flow patterns were measured in six cross-sections around the middle bend, and the bed topography was measured in the whole reach. Main reach-averaged characteristics of this bend are summarized in Table 3.

Table 3 Estimation of geometrical parameters in some natural meandering rivers (Blanckaert et al., 2009)

Label	Q $[m^3\ s^{-1}]$	B [m]	H [m]	U $[m\ s^{-1}]$	R [m]	C $[m^{1/2}\ s^{-1}]$	R/B [-]	R/H [-]	B/H [-]
Ledra river (Italy)	18	15	1.5	0.8	45	22.8	3	30	10

The scour factor A/R was directly derived from the measured bed topography. Model results are illustrated in Figure 5 where the sections with maximal $v_{n,surf,ref}$ have been indicated in the three bends. The maximum predicted values of max($v_{n,surf,ref}$) were 0.11 m s^{-1}, 0.13 m s^{-1}, and 0.14 m s^{-1} (see Figure 5), respectively. The predicted value in the middle bend agrees satisfactorily with the field measurements around cross-section 2 which were within the range –0.11 to –0.20 m s^{-1}.

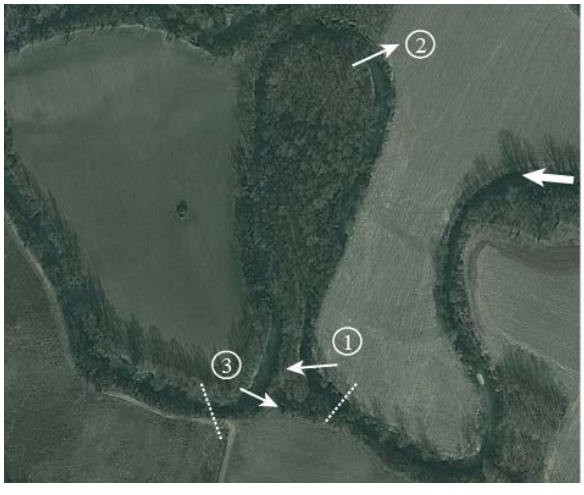

Section	$v_{n,surf,ref}$ $[m\ s^{-1}]$
①	0.11
②	−0.13
③	0.14

Figure 5 Bend on the Ledra River (Italy, Image: Google Earth) and maximal $v_{n,surf,ref}$ computed with Blanckaert and de Vriend's model (2003; 2010). The dashed lines indicate the domain of the numerical simulation. The white arrows indicate the location of the maximum values of $v_{n,surf,ref}$.

From the simulation results, the minimum air discharge required to counteract the curvature-induced

secondary flow for the investigated water discharge is estimated according to Eq. 3. Results for the two investigated bends are summarized in Table 4.

Table 4 Estimation of required air discharges for the investigated sharp bend.

Label	$max(v_{n,surf,ref})$ $[m\ s^{-1}]$	q_a $[dm^3\ s^{-1}\ m^{-1}]$	L $[m]$	Qa $[m^3\ s^{-1}]$
Ledra river (Italy)	0.14	0.07	671	0.04

L is the length of the required air-line source and Q_a the required air discharge.

The required air discharge in the Ledra is relatively low compared to other environmental application of bubble screens. Lake destratification, for example, typically requires air discharges ranging from 0.01 to 1.2 $m^3\ s^{-1}$ (Wüest et al., 1992; Sahoo and Luketina, 2006; Boegman and Sleep, 2012). Neto et al. (2007) applied a bubble screen to increase the dissolved oxygen level in an ice-covered river with an oxygen flow rate of 0.87 $m^3\ s^{-1}$ on an air-line source length of 52 m. It can be concluded that, the bubble-screen technique can represent a good alternative to influence the flow field and the bed morphology in rivers with a non-prohibitive cost as compared to other environmental applications.

7 CONCLUSION

A bubble screen, placed near the outer bank in a sharply curved flume, can produce a bubble-induced secondary flow that is able to redistribute the flow pattern, the bed shear stress distribution and consequently the bend morphology.

Three types of experiments were performed under different conditions of bed morphology (fixed horizontal bed vs. developed bed) and sediment transport (fixed bed, clear-water scour, live bed) to highlight the processes involved in the interaction between the bubble screen, the main velocity, the secondary flow, the sediment transport and the bed morphology.

The bubble screen is found to be efficient if the maximum inward transverse velocities at the water surface produced by the bubble screen are higher than the maximal outward transverse velocities induced by the bend curvature. Moreover, this condition has to be satisfied over the whole length of the bend.

Based on this criterion, a straightforward method to evaluate the efficiency of a bubble screen to redistribute the flow patterns and the morphology has been proposed, and illustrated by means of an application in a real river. The minimum air discharges required to counteract the maximal transverse velocities induced by the curvature are relatively low as compared to other types of environmental applications of the bubble screens.

The bubble-screen technique has the potential to be applied as a countermeasure for reducing bed scour and inner bank sediment deposition in curved river reaches. These results are based on experiments in a flume with fixed banks, and no measurements could be made in the region between the bubble screen and the adjacent bank. Therefore, the application of the bubble screen technique should at present be limited to configurations with fixed banks.

ACKNOWLEDGEMENT

This research was financially supported by the Swiss National Science Foundation under grants 200021-125095. The second author was partially funded by the Chinese Academy of Sciences Visiting Professorship for Senior International Scientists, grant number 2011T2Z24, and by the Sino-Swiss Science and Technology Cooperation for the Institutional Partnership Project, grant number IP13_092911.

References

Blanckaert K. and de Vriend H. J., 2003. Nonlinear modeling of mean flow redistribution in curved open channels, Water Resources Research, 39(12), 1375-1381.

Blanckaert K., Buschman F. A., Schielen R. and Wijbenga J. H. A., 2008. Redistribution of velocity and bed-shear stress in straight and curved open channels by means of a bubble screen: Laboratory experiments. Journal of Hydraulic Engineering, 134(2), 184-195.

Blanckaert K., Schnauder I., Sukhodolov A., van Balen W., and Uijttewaal W. S. J., 2009. Meandering: field

experiments, laboratory experiments and numerical modeling, Proc. Of the 6th IAHR Symposium on River, Coastal and estuarine Morphodynamics, Santa Fe, Argentina.
Blanckaert K., 2010. Topographic steering; flow recirculation, velocity redistribution, and bed topography in sharp meander bends, Water Resources Research, 46, W09506, doi:10.1029/2010JF001806.
Blanckaert, K. and de Vriend H. J., 2010. Meander dynamics : A nonlinear model without curvature restrictions for flow in open-channel bends, Journal of Geophysical Research-Earth Surface, 115, F04011, doi :10.1029/2009JF001301.
Boegman L. and Sleep S., 2012. Feasibility of bubble plume destratification of central lake Erie, Journal of Hydraulic Engineering-ASCE, 138(11), 985-989.
Brevik I., 1977. Two-dimensional air-bubble plume. Journal of the Waterway Port Coastal and Ocean Division, 103(1), 101-115.
Brevik I. and Kristiansen O., 2002. The flow in and around air-bubble plumes. International Journal of Multiphase Flow, 28(4), 617-634.
Camporeale C., Perona P., Porporato A. and Ridolfi L., 2007. Hierarchy of models for meandering rivers and related morphodynamic processes, Reviews of Geophysics, 45(1), doi:10.1029/2005RG000185.
de Vriend H. J., 1977. Mathematical-model of steady flow in curved shallow channels, Journal of Hydraulic Research, 15(1), 37-54.
de Vriend, H. J., 1981. Velocity redistribution in curved rectangular channels, Journal of Fluid Mechanics, 107(6), 423-439.
de Vriend H. J. and Struiksma N., 1984. Flow and bed deformation in river bends, in River Meandering, edited by C. M. Elliot, pp. 810–828, ASCE, New Orleans, Louisiana, ISBN 0-87262-393-9.
Dietrich W. E. and Smith J. D., 1983. Influence of the point bar on flow through curved channel, Water Resources Research, 19(5), 1173-1192.
Dugué V., Blanckaert K., Chen Q., and Schleiss A. J. (2013). Reduction of bend scour with an air-bubble screen – morphology and flow patterns, International Journal of Sediment Research, 28(1), 15-23.
Dugué V. 2013. Influencing river morphodynamics by means of a bubble screen: Application to open-channel bends. PhD-thesis N° 5676, Ecole Polytechnique Fédérale de Lausanne, Switzerland.
Engel F. L. and Rhoads B. L., 2012. Interaction among mean flow, turbulence, bed morphology, bank failures and channel planform in an evolving compound meander loop, Geomorphology, 163, 70-83.
Fanneløp T. K., Hirschberg S. and Küffer J., 1991. Surface current and recirculating cells generated by bubble curtains and jets. Journal of Fluid Mechanics, 229, 629-657.
Fischer-Antze T., Olsen N. R. B. and Gutknecht D., 2008. Three-dimensional CFD modeling of morphological bed changes in the Danube River, Water Resources Research, 44(9).
Frothingham K. M. and Rhoads B. L., 2003. Three-dimensional flow structure and channel change in an asymmetrical compound meander loop, Embarras River, Illinois, Earth Surface Processes and Landforms, 28(6), 625-644.
Hurther D. and Lemmin U., 1998. A constant-beam-width transducer for 3D acoustic Doppler profile measurements in open-channel flows, Measurement Science & Technology, 9(10), 1706-1714.
Ikeda S., Parker G. and Sawai K., 1981. Bend theory of river meanders. Part 1. Linear development, Journal of Fluid Mechanics, 112(11), 363-377.
Johannesson H. and Parker G., 1989. Velocity redistribution in meandering rivers, Journal of Hydraulic Engineering-ASCE, 115(8), 1019-1039.
Lemmin U. and Rolland T., 1997. Acoustic velocity profiler for laboratory and field studies, Journal of Hydraulic Engineering-ASCE, 123(12), 1089–1098.
Milgram J. H., 1983. Mean flow in round bubble plumes. Journal of Fluid Mechanics, 133, 345-376.
Nanson R. A., 2010. Flow fields in tightly curving meander bends of low width-depth ratio, Earth Surface Processes and Landforms, 35(2), 119-135.
Nelson J. E., 1988. Mechanics of flow and sediment transport over non-uniform erodible beds, PhD-thesis, University of Washington, Seattle.
Neto I. E. L., Zhu D. Z., Rajaratnam N., Yu T., Spafford M. and McEachem P., 2007. Dissolved oxygen downstream of an effluent outfall in an ice-covered river: Natural and artificial aeration, Journal of Environmental Engineering-ASCE, 133(11), 1051-1060.
Odgaard A. J., 1981. Transverse bed slope in alluvial channel bends, Journal of the Hydraulics Division-ASCE, 107(12), 1677-1694.
Odgaard A. J., 1989. River-Meander model. I. development, Journal of Hydraulic Engineering-ASCE, 115(11), 1433–1450.
Ottevanger W., Blanckaert K. and Uijttewaal W. S. J., 2012. Processes governing the flow redistribution in sharp river bends, Geomorphology, 163, 45-55.
Ottevanger W., Blanckaert K., Uijttewaal W.S.J. and de Vriend H.J., 2013. Meander dynamics: A reduced order non-linear model without curvature restrictions for flow and bed morphology, Journal of Geophysical Research – Earth Surface, doi: 10.1002/jgrf.20080
Riess I. R. and Fanneløp T. K., 1998. Recirculating flow generated by line-source bubble plumes. Journal of Hydraulic Engineering, 124(9), 932-940.
Rozovskii I. L., 1957. Flow of water in bends of open channels, Academy of Sciences of the Ukrainian SSR, Kiev

1957; Israel program for Scientific Translations, Jerusalem, 1961.
Rüther N. and Olsen N. R. B., 2007. Modelling free-forming meander evolution in a laboratory channel using three-dimensional computational fluid dynamics, Geomorphology, 89(3-4), 308-319.
Sahoo G. B. and Luketina D., 2006. Response of a tropical reservoir to bubbler destratification, Journal of Environmental Engineering-ASCE, 132(7), 736-746.
Sukhodolov A. N., 2012. Structure of turbulent flow in a meander bend of a lowland river, Water Resources Research, 48, W01516, doi: 01510.01029/02011WR10765.
van Balen W., Uijttewaal W. S. J. and Blanckaert K., 2009. Large-eddy simulation of a mildly curved open-channel flow, Journal of Fluid Mechanics, 630, 413-442.
van Balen W., Blanckaert K. and Uijttewaal W. S. J., 2010a. Analysis of the role of turbulence in curved open-channel flow at different water depths by means of experiments, LES and RANS, Journal of Turbulence, 11(12), 1-34.
van Balen W., Uijttewaal W. S. J. and Blanckaert K., 2010b. Large-eddy simulation of a curved open-channel flow over topography, Physics of Fluids, 22, 075108(7).
Wen J. and Torrest R. S., 1987. Aeration-induced circulation from line sources. 1. Channel flows. Journal of Environmental Engineering, 113(1), 82-98.
Wüest A., Brooks N. H. and Imboden D. M., 1992. Bubble plume modeling for lake restoration, Water Resources Research, 28(12), 3235-3250.
Yeh K. C. and Kennedy J. F., 1993. Moment model of nonuniform channel-bend flow. 1. Fixed beds, Journal of Hydraulic Engineering-ASCE, 119(7), 776-795.
Zeng J., Constantinescu G., Blanckaert K. and Weber L., 2008. Flow and bathymetry in sharp open-channel bends: Experiments and predictions, Water Resources Research, 44. W09401, doi:10.1029/2007WR006303(9).
Zolezzi G. and Seminara G., 2001. Downstream and upstream influence in river meandering. Part 1. General theory and application to overdeepening, Journal of Fluid Mechanics, 438, 183-211.